

# Physicochemical Properties of New Silicone Alternatives Unraveled by Experimental and Molecular Modeling Techniques

Tiago Ferreira,<sup>||</sup> Diana Rocha,<sup>||</sup> David Freitas, Jennifer Noro, Mariana de Castro, Catarina Roque, Diana Guimarães, Ana Loureiro, Carla Silva, Artur Cavaco-Paulo, and Tarsila G. Castro\*



Cite This: *Ind. Eng. Chem. Res.* 2024, 63, 9715–9731



Read Online

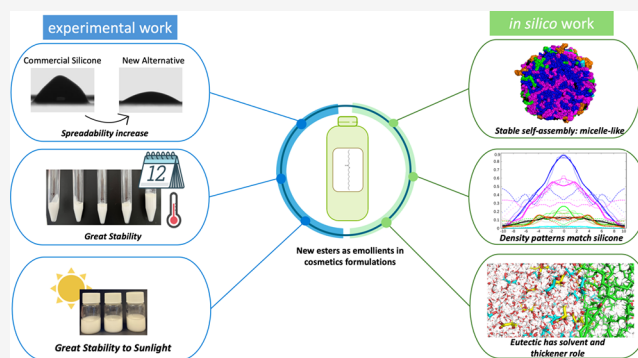
ACCESS |

Metrics & More

Article Recommendations

Supporting Information

**ABSTRACT:** The cosmetic industry has recognized an increasing demand for environmentally sustainable solutions due to the classification of certain commonly used components as bio-accumulative and hazardous. The European Union has implemented restrictions on the utilization of some components, including silicones, which limit their concentration. The present investigation intends to find new solutions for cosmetic formulations by combining molecular dynamics simulations with an array of experimental techniques to fully characterize silicone alternatives. The novelty of the work relies on the addition of an organic deep eutectic solvent and ester-based emollients in place of conventional silicones. These formulations exhibit great stability when adding a 15% weight-to-weight glycerol:lactic acid eutectic mixture, acting as both a solvent and a thickener-like behavior. The novel esters were incorporated into a cosmetic-based formulation and tested to comprehend their physicochemical properties, stability, and molecular distribution. Widely used silicones and commercial silicone alternatives were also tested for comparison purposes. Based on our research findings, it has been determined that the new emollients, specifically decyl heptanoate, decyl octanoate, and decyl decanoate, conferred great stability and performance to the tested formulations. The formulations comprising the novel esters exhibit superior spreadability compared to those including silicones and are comparable to formulations using commercially available alternatives. The modeling techniques applied disclose the molecular features behind the component's distribution, helping to differentiate the formulations where the key molecule—silicon or alternative—has induced phase separation or not. This creates the opportunity to optimize the entire production process by foreseeing the function of new esters in a formulation.



## 1. INTRODUCTION

The skin, our body's largest organ, covers almost the entire surface of the human body and thus serves as an extremely vital and defensive barrier against dehydration and other environmental factors. To perform its functions, the skin must be in good condition. Properly hydrated skin is more resistant to external impacts, and ages more slowly than skin that is dehydrated.<sup>1,2</sup> This is where cosmetic and cosmeceutical products come in to tackle varied aspects. Skin protection, sunscreen, antiacne, antiwrinkle, and antiaging compositions are designed for many types of skin disorders by utilizing a variety of natural or synthetic components. The claims made by the product as well as the efficacy given by the components affect the success of a cosmetic formulation. Water, emollients, emulsifiers, humectants, oils, alcohols, active agents, preservatives, perfumes, and other ingredients make up complex cosmetic formulations.

In cosmetic formulations, emollients are the second most important element after water, with concentrations ranging from 3 to 20% (w/w).<sup>3</sup> These products are multifunctional

ingredients used in cosmetology, dermo cosmetology, and dermatology to support a variety of formulation claims that play a role in the maintenance of the skin's soft, smooth, and malleable appearance. These components function by lingering on the skin's surface or in the stratum corneum to act as a lubricant, reducing flaking, and improving the skin's look.<sup>3,4</sup> They decrease the friction coefficient of the emulsion and affect its spreading properties when applied to the skin due to their lubricating qualities.<sup>5,6</sup> A formulation's spreadability/smoothness provides a variety of sensory properties and is one of the aspects that the consumer analyzes instantly at the time of purchase, which might influence the product's acceptability.<sup>7,8</sup>

**Received:** March 11, 2024

**Revised:** May 14, 2024

**Accepted:** May 14, 2024

**Published:** May 22, 2024



Regarding consumer needs, the environmental issue demands products formulated with biobased raw materials. The characteristic of silicones, such as cyclomethicones, that sets them apart is their light and pleasant touch, attributed to the strength of the Si–O bond, which imparts excellent thermal, chemical, and biological stability. However, this strength also hinders the biodegradability of silicone oils, leading to significant potential for bioaccumulation. The compound known as decamethylcyclopentasiloxane has been classified as a vPvB (very persistent and very bioaccumulative) chemical. The increased severity of environmental concerns has resulted in stricter regulations within the cosmetic industry. As a result, the European Union has implemented limitations on the utilization of decamethylcyclopentasiloxane and other silicones in rinse-off products, setting the maximum allowable concentration at 0.1 wt % starting from January 2020.<sup>9</sup>

The chemical structure, molecular weight, spreading characteristics, viscosity, surface tension, volatility, and lubricity of an emollient all contribute to its perception in the formulation.<sup>9,10</sup> Emollients have a wide range of chemical structures, including hydrocarbons, fatty alcohols, esters, and silicone derivatives. Particularly, esters and silicones are hydrophobic ingredients that constitute part of the oil phase in cosmetic emulsions.<sup>6</sup> Esters are a broad class of chemicals, synthesized from alcohols and fatty acids, that can be used to replace silicones in cosmetic emulsions as either an emollient or an emulsifier. There are several possible combinations, making ester-based emollients a particularly versatile category with a wide range of properties. They can be used to alter the consistency of a formulation or improve the spreadability of sunscreens, for example.<sup>7</sup> Rheological and texture analysis of cosmetics emulsions are the most common approaches to characterize and evaluate new esters (emollients), which give important information about the product flow behavior and spreadability, as well as firmness and consistency.

Because synthetic silicones are highly insoluble molecules, they have been a target for replacement due to concerns about bioaccumulation in wastewater and, more importantly, the use of aggressive surfactants to incorporate them into these formulations or to cleanse the product from the hair or skin.<sup>11,12</sup> The present study aimed to evaluate the effect of various esters as silicone alternatives in a cosmetic-based formulation. For this purpose, three commercial silicones—cyclopentasiloxane, dimethicone 5, and dimethicone 10 cst—and three commercial alternatives to silicones—cetiol CC, cetiol soft, and cetiol C5—are used to compare their effect and properties against a small collection of esters, previously produced by us.<sup>13</sup> The formulations were characterized, mainly regarding rheologic properties, texture analysis, spreadability contact angle, and physical–chemical properties.

Computational simulations, which have gained attention as an important tool within scientific research and companies' workflow for their R&D processes, were employed herein to disclose the molecular distribution and stability of the cosmetic-based formulation incorporating a silicone, a commercial alternative, and the selected ester alternatives. These simulations highlight the molecular processes and interactions behind formulations' formation and can be used to streamline the R&D process involved in the production of novel products.<sup>14,15</sup> Computer simulations in cosmetics may not be as widespread as in other fields, but ongoing research and development is using them for formulation design. Our work contributes to elucidating how in silico techniques can

aid in cosmetics design, by establishing new protocols and analysis.

## 2. MATERIALS AND METHODS

### 2.1. Preparation of Cosmetic-Based Formulations.

Thirteen water-in-oil (W/O) emulsions were prepared as typical cosmetic creams (composition in Table 1), each differing only in the silicone or alternative added, except for the base formulation (BF) (control, without silicone or alternative).

**Table 1. List of Ingredients Used for the Water-in-Oil Cosmetic-Based Formulation<sup>a</sup>**

	ingredients	content (%, w/w)	function
part A (aqueous phase)	distilled water	75.2	solvent
	euxyl PE 90/ 10	1	preservative
	xanthan gum	0.8	thickener
part B (oil phase)	NADES 4:1 (pH = 5.7)	15	thickener-like agent, solvent, and pH adjuster
	EasyNov	3	emulsifier
	sweet almond oil	1	emollient
	silicone/alternative 4		emollient

<sup>a</sup>Euxyl PE 90/10: phenoxyethanol and ethylhexylglycerin; xanthan gum: polysaccharide of D-glucose, D-mannose, and D-glucuronic acid; NADES (4:1) glycerol:lactic acid; EasyNov: octyldodecanol, octyldodecyl xyloside, and PEG-30 dipolyhydroxystearate; sweet almond oil: trioleylglycerol (triolein).

The silicone or alternatives, each one incorporated at a concentration of 4% (w/w) in the emulsion, are listed in Table 2, identified by a code. To prepare the formulations, the aqueous phase was performed in a T25 Digital Ultra-Turrax IKA (11,000 rpm, 2 min) and incorporated into the oil phase under agitation (500 rpm) for 5 min, using a mechanical propeller, and left 5 min at 200 rpm. The glycerol: lactic acid (4:1) natural deep eutectic mixture (NADES) (15% w/w) was incorporated into the oil phase functioning as a thickening-like agent, solvent, and pH adjuster. Various concentrations of NADES were tested (5% to 30%), but a stable cosmetic formulation was obtained only when 15% of this mixture was applied. The stability of formulations was assessed throughout time by considering their organoleptic and sensory qualities as well as sensorial, rheologic, and textural assessments.

**2.2. Physicochemical Characterization of Cosmetic Formulations.** **2.2.1. pH.** pH measurements were performed by using an analogic pH meter; all measurements were performed at room temperature.

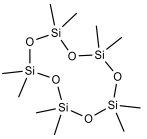
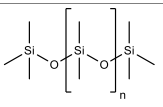
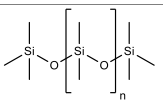
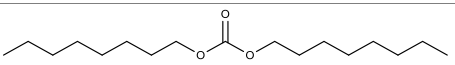
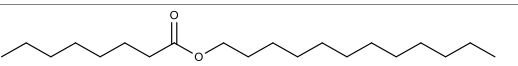
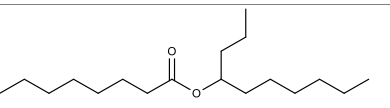
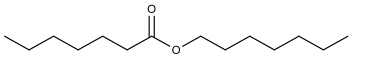
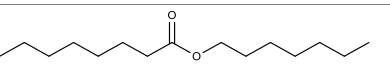
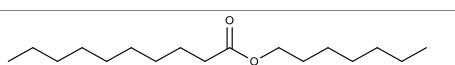
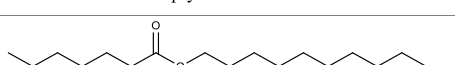
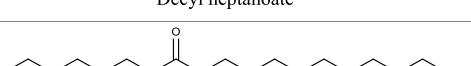
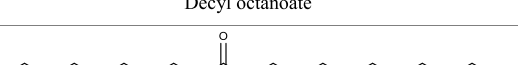
**2.2.2. Density.** The density was measured in duplicate by weighing 25 mL of formulations inside a 25.00 ± 0.01 mL pycnometer; the final density was obtained by calculation of the quotient between the mass and the volume of the solvent.

**2.2.3. Refractive Index.** The refractive indices of samples were measured in duplicate using a Bellingham and Stabley Abbe Refractometer (model 60/ED).

**2.2.4. Conductivity.** The conductivity was measured using a Thermo Scientific benchtop meter (Orion Versa Star Pro); all measurements were taken at 25 °C and atmospheric pressure.

**2.2.5. Particle Size, Polydispersity (PDI), Surface Charge.** The particle size, PDI, and surface charge, expressed as zeta-potential ( $\zeta$ ) values, of the formulations were evaluated in a

Table 2. Name and Structure of Silicones and Alternatives (Commercial and Developed) Used As Well As the Code Applied to Each Developed Formulation

	Name and structure	Formulations Code
Control	Base formulation	BF
		BF+CP
	Decamethylcyclopentasiloxane	
Commercial Silicones		BF+D5
	Dimethicone 5 cst	
		BF+D10
	Dimethicone 10 cst	
Commercial Alternatives		BF+CC
	Cetiol CC (Dicaprylyl Carbonate)	
		BF+C5
	Cetiol C5 (Coco-Caprylate)	
		BF+CS
	Cetiol Sensoft (Propylheptyl Caprylate)	
		BF+A1
	Heptyl heptanoate	
		BF+A2
	Heptyl octanoate	
		BF+A3
	Heptyl decanoate	
New Alternatives		BF+A4
	Decyl heptanoate	
		BF+A5
	Decyl octanoate	
		BF+A6
	Decyl decanoate	

Malvern Zetasizer NS (Malvern Instruments) at room temperature.

**2.3. Stability Tests.** The formulations developed were submitted to some testing to infer their stability along time. For this, cosmetic formulations were stored at different temperatures,  $-12$ ,  $4$ ,  $25$  and  $37$  °C, for 12 months. The organoleptic characteristics of the preparations, such as odor, appearance, and color, were evaluated by visual inspection, the pH was measured, and centrifugation tests (3000 rpm (1200G) for 30 min) were made one time per month aiming to evaluate the occurrence of phase separation. The extreme temperature stability test, carried out by cycling of cool and heat processes, was also performed. For this, samples were subjected to 3 cycles of extreme temperatures, with each cycle consisting of placing the samples at  $-12$  °C for 24 h followed by 24 h at room temperature. A visual assessment of the organoleptic qualities, pH measurement, and centrifugation test was done at the end of each cycle. The stability of the formulations to sunlight was also evaluated. Each formulation was prepared and packaged in glass and plastic containers, both uncovered and covered with aluminum foil, to avoid direct contact with sunlight on the samples. All samples were placed near a window to evaluate their stability when exposed to natural sunlight.

**2.4. Contact Angle Measurements.** The contact angle between the samples and a solid support was evaluated to investigate the spreadability of the cosmetic formulations through the drop method (DataPhysics OCA 20) using poly(methyl methacrylate) (PMMA) plates as solid support. This support is commonly used in cosmetics for in vitro SPF (sun protection factor) determination and has several advantages over artificial skin for our purposes: it is less expensive, easier to handle in terms of surface preparation and cleaning, reproducible in terms of surface chemistry and roughness, and reusable.<sup>6</sup> A drop of each formulation ( $10$   $\mu\text{L}$ ) was dispensed by a syringe at  $5$   $\mu\text{L}/\text{s}$  onto the solid support and then spread onto it.

A high-speed camera captured the evolution of the contact angle between the drop and the solid support immediately after deposition and throughout the spreading process. The contact angle for each sample was measured every 30 s for 2 min. The results are the averages of three reproducible experiments performed at room temperature.

**2.5. Texture Analysis.** The texture analysis was performed using a texturometer, a Stable Micro Systems TA.HDplus. The equipment is composed of two probes: Back Extrusion rig A/BE 35 mm and TTC Spreadability rig HDP/SR. The extrusion test was conducted with a Back Extrusion Rig A/BE probe with a disc diameter of 35 mm and a Back Extrusion container loaded with formulations until 75% of its capacity was reached to evaluate different parameters such as firmness, index of viscosity, consistency, and cohesiveness. The probe penetrated each formulation to a depth at a predetermined speed and depth, which results in a predefined period of recovery between the end of the first compression and the beginning of the second, resulting in a force (g) versus time (t) graph.<sup>16</sup> Consistency is given by the area under the positive curve. Firmness is obtained from the maximum value of the positive curve, index of viscosity from the area under the negative curve and cohesiveness from the maximum value of the negative curve (Figure 1).<sup>17</sup> The spreadability test was conducted on a TTC Spreadability Rig (HDP/SR) attachment (Stable Microsystems, Surrey, UK) with a P/45C Perplex, with a depth of 60

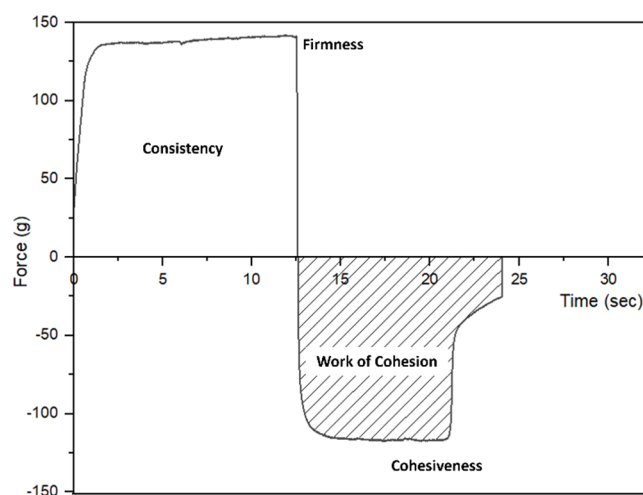


**Figure 1.** Typical plot of texture analysis with data graph and its interpretation (sample used: BF+CS).

mm, test speed of  $10$   $\text{mm s}^{-1}$ , and contact force of  $10$  g, to evaluate the work of the shear parameter. The work of the shear is given from the area under the positive curve. The values of work of shear are highly correlated with the spreadability of the formulation. The lowest work of shear presented the best spreadability.<sup>18</sup> All measurements were run in duplicate at room temperature with a load cell of 2 kg.

**2.6. Rheological Analysis.** All rheological tests were performed using a Discovery Hybrid Rheometer (TA Instrument) at  $25$  °C. The temperature of the samples was kept constant to ensure an efficient determination of the viscosity as small variations in this parameter could result in significant changes of this parameter. The rheological evaluation was performed using a stainless-steel cone–plate geometry of 20 mm,  $2.006^\circ$  cone plate, and a gap of  $59$   $\mu\text{m}$ . Measurements were made in duplicate, and a fresh sample was loaded for each run.

In a flow sweep test, samples' shear stress and viscosity were measured at varying shear rates. The shear rate was increased from  $0.01$  to  $1000$   $\text{s}^{-1}$ , then decreased to  $0.01$   $\text{s}^{-1}$ , and finally increased once again to  $1000$   $\text{s}^{-1}$  (logarithmic mode, 5 points per decade), and the values from the third sweeps were considered for analysis. The first applied stress cycle served to discard the primary viscosity of the samples. The linear viscoelastic region (LVR) of each sample was identified in an oscillatory strain sweep test at a fixed frequency of 1 Hz, and increasing strain from 13 to 8000% was carried out. These experiments enabled obtaining the LVR, corresponding to properties independent from the applied strain amplitude and the viscoelastic moduli only depend on time or frequency.<sup>19</sup> After the flow sweep test, an oscillatory frequency sweep test was performed, with angular frequency ranging from 0.1 to 10 rad/s at a strain of 4%, within the LVR as determined from the previous strain sweep test.<sup>20</sup> Results were plotted as the average of the duplicate measurements.

## 2.7. Molecular Dynamics Simulations and Analysis.

**2.7.1. Systems Design.** The systems under study are composed of the ingredients listed in Table 1, where the emollient is a known cosmetic silicone, a commercial alternative, or a selected developed ester (Table 2). These were first drawn and prepared with the help of both MarvinSketch<sup>21</sup> and LigParGen<sup>22</sup> in order to have the optimized potentials for liquid simulations (OPLS) parameters for the simulation. For

EasyNov, Euxyl PE 90/10, and almond oil, only the preponderant ingredient was considered for molecular simulations. In the case of EasyNov, the representative molecule was the octyldodecanol, for Euxyl PE 90/10, both phenoxyethanol and ethylhexylglycerin were considered, and to represent the almond oil, only the trioleylglycerol (triolein) was inserted in the simulation box.

Systems were assembled via the random placing of all elements in a 15625 nm<sup>3</sup> volume simulation box, thus creating adequate conditions for the accommodation of all molecules and for the self-aggregation process (Figure 2). After the

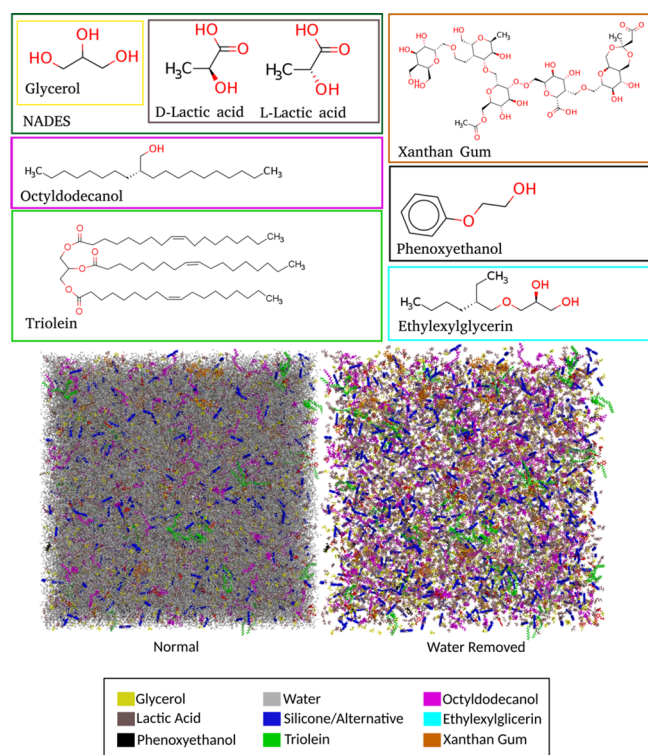


**Figure 2.** Example of an input system with a simulation box containing the ingredients of the formulation composed of 75.2% water, 1% of ethylhexylglycerin and phenoxyethanol (Euxyl PE 90/10), 0.8% of xanthan gum, 15% of NADES (glycerol:lactic acid), 3% of octyldodecanol (EasyNov), 1% of triolein (sweet almond oil), and 4% of silicone alternative, with the respective color description.

initialization step, where the pressure barostat is on (NPT ensemble), the box was adjusted to a volume of 8000 nm<sup>3</sup>. This method was considered competent as it represented very well the final systems' supramolecular structures and was proven to reach stability fairly easily for previous formulations studied by us in a time frame of 100 ns.<sup>2,3</sup>

**2.7.2. MD Simulations and Analysis.** The systems were submitted to energy minimization using a maximum of 50,000 steps using the steepest descent method. Both canonical (NVT) and isothermal–isobaric (NPT) ensembles were used for the initialization, for 100 ps each, only to relax hydrogen atoms and water molecules. These ensembles are important to prepare all systems for a stable and reliable simulation later on. NVT maintains a constant number of particles ( $N$ ), volume ( $V$ ), and temperature ( $T$ ) while NPT keeps the number of particles ( $N$ ), pressure ( $P$ ), and temperature ( $T$ ) constant.  $V$ -rescale algorithm<sup>24,25</sup> was used to set all systems at room temperature (298 K  $\approx$  25 °C), and the pressure was regulated

at 1 atm with the Parrinello–Rahman<sup>25,26</sup> barostat. The following coupling constants were considered:  $\tau_T = 0.10$  ps and  $\tau_P = 2.0$  ps. Having all the systems prepared, production runs were started. MD simulations were performed for 100 ns using the NPT ensemble, without position restraints.

Using the built-in tools provided by GROMACS 2021.2,<sup>27,28</sup> partial densities across the simulation box were calculated at 1 ns as an initial time ( $t_0$ ) and with a 25 ns time-interval afterward, using the density tool. As per our previous protocol,<sup>23</sup> following each molecule's partial density across the box during simulation time is a proper way to follow equilibration and molecular distribution.

Subsequent analyses were conducted for the last 15 ns of simulation time to guarantee the observation of the desired properties, when the systems are equilibrated. The global density of each system/formulation, in turn, was calculated using the energy module. Additionally, solvent-accessible surface area (SASA) and diffusivity—from the mean square displacement (MSD) analysis—were also taken using the tools provided by the GROMACS environment.

Clustering analysis was performed to determine the most representative molecular organization also for the last 15 ns of simulation time. This is achieved via a single-linkage method which clustered structures below an root mean square deviation (RMSD) cutoff, generating more or less populated clusters and, within the largest cluster, finds a middle structure (that minimizes the RMSD variance) that is the most representative of the whole simulation. Although each ingredient will have different RMSD ranges, indicating more/less flexibility and mobility, this is an attempt to have a graphical representation of the system's final state. By default, the cluster's RMSD cutoff is 0.1 nm (for peptides/proteins), however due to the nature and complexity of our systems, wide RMSD is expected, and we increased this value to 1.0 nm.

All simulations were performed using the GROMACS 2021.2 version, in double precision, with the OPLS<sup>29,30</sup> force field. The Lennard–Jones interactions were truncated at 1.0 nm and we used the particle mesh Ewald<sup>31</sup> method for electrostatic interactions, with a cutoff of 1.0 nm. Data were plotted using GNUPLOT<sup>32</sup> and Grace.<sup>33</sup>

### 3. RESULTS AND DISCUSSION

**3.1. Physicochemical Characterization of Cosmetic Formulations.** The physical–chemical characterization of cosmetic formulations included the pH, density, conductivity, and refractive index determination (Table 3). Because cosmetic formulations' application is the skin, the formulation pH is a key parameter. Human skin's pH varies depending on the body region, having an average value of 5.5. All cosmetic formulations under consideration own pH values between 4.8 and 4.9, which is an acceptable value for skin applications. The density of the formulations ranges from 1.00 to 1.03 g/mL, indicating that there are no density variations between the samples and the BF. The conductivity is commonly used to determine the type of emulsion and evaluate the emulsion stability. The aqueous phase usually contains some electrolytes, but the oil phase does not. High conductivity values (higher than 50  $\mu\text{S cm}^{-1}$ ) indicate o/w emulsions, whereas low conductivity values ( $<1 \mu\text{S cm}^{-1}$ ) indicate w/o emulsions<sup>34</sup> because the typical electrolytic conductivity of the oil phase is 100 or 1000 times smaller than the conductivity of the aqueous phase as the mobility of ions is restricted due to the

**Table 3. Physicochemical Properties of the Different Formulations Tested: pH, Density ( $\rho$ ), Conductivity ( $\sigma$ ), Refraction Index ( $nD$ ), and Diffusivity ( $D$ )<sup>b</sup>**

formulations code	pH	$\rho$ (g/mL)	$\sigma$ ( $\mu\text{S cm}^{-1}$ )	$nD$	$D$ ( $10^{-5}$ cm <sup>2</sup> /s) <sup>aa</sup>	$\rho$ (g/mL) <sup>a</sup>
BF	4.983	1.017	0.158	1.364		
BF+CP	4.871	1.031	0.394	1.367		
BF+D5	4.940	1.021	0.384	1.367	0.055 ± 0.006	1.006 ± 0.004
BF+D10	4.829	1.000	0.107	1.366		
BF+CC	4.934	1.007	0.235	1.374	0.078 ± 0.025	1.003 ± 0.017
BF+C5	4.924	1.013	0.168	1.378		
BF+CS	4.891	1.009	0.593	1.377		
BF+A1	4.916	1.026	0.832	1.381		
BF+A2	4.805	1.024	0.600	1.389	0.112 ± 0.016	1.001 ± 0.012
BF+A3	4.996	1.019	1.070	1.355	0.138 ± 0.008	1.002 ± 0.016
BF+A4	4.898	1.015	0.451	1.371		
BF+A5	4.968	1.021	0.530	1.369	0.091 ± 0.031	1.001 ± 0.008
BF+A6	4.973	1.026	0.253	1.371	0.112 ± 0.040	1.001 ± 0.011

<sup>a</sup>In silico calculations. <sup>b</sup>Experimental measurements were performed at 25 °C. BF: base formulation, BF+CP: base containing decamethylcyclopentasiloxane, BF+D5: base containing dimethicone 5 cst; BF+D10: base containing dimethicone 10 cst; BF+CC: base containing cetiol CC; BF+C5: base containing cetiol C5; BF+CS: base containing cetiol sensoft; BF+A1: base containing heptyl heptanoate; BF+A2: base containing heptyl octanoate; BF+A3: base containing heptyl decanoate; BF+A4: base containing decyl heptanoate; BF+A5: base containing decyl octanoate; BF+A6: base containing decyl decanoate. In silico diffusivity ( $D$ ) was measured for the silicone or silicone alternative present in the formulation (D5, CC, A2, A3, A5, A6).

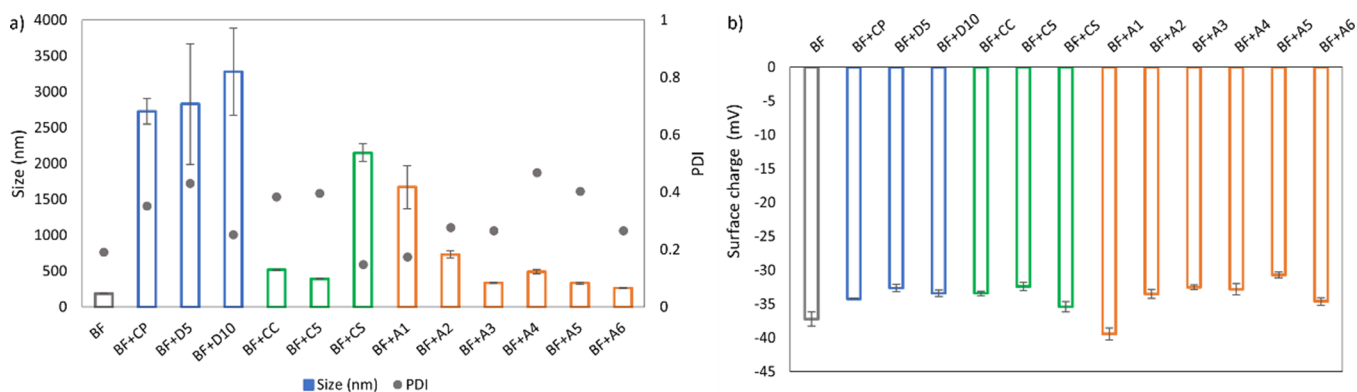


**Figure 3.** Particle size and PDI (a), and surface charge (b) of cosmetic formulations; BF: base formulation, BF+CP: base containing decamethylcyclopentasiloxane, BF+D5: base containing dimethicone 5 cst; BF+D10: base containing dimethicone 10 cst; BF+CC: base containing cetiol CC; BF+C5: base containing cetiol C5; BF+CS: base containing cetiol sensoft; BF+A1: base containing heptyl heptanoate; BF+A2: base containing heptyl octanoate; BF+A3: base containing heptyl decanoate; BF+A4: base containing decyl heptanoate; BF+A5: base containing decyl octanoate; BF+A6: base containing decyl decanoate.

surrounding strongly insulating oil that disconnects the water network.<sup>35</sup>

The BF has the lowest conductivity ( $0.158 \mu\text{S cm}^{-1}$ ) compared to the formulations containing the emollients. Conductivity increased with the addition of silicones and alternatives (commercial and newly developed). The maximum conductivity ( $1.070 \mu\text{S cm}^{-1}$ ) is found in the BF+A3 formulation containing heptyl decanoate. Regarding the refractive index data, one may observe that all of the samples display similar values ( $\sim 1.3$ ).

Regarding molecular simulations, the diffusivity was measured by MSD analysis, aiming to infer the molecular motion of the silicone or alternative, individually, among the other components. This can be an implicit way to look at compounds' spreadability, by understanding how fast the molecules spread in the mixture. These values will be further addressed in Section 3.5.1. In addition, the calculated density correlates very well with experimental data, reinforcing the ability of GROMACS and the OPLS force field, which is

optimized for organic molecules and liquid simulations, to represent the physics of these types of systems.

The particle size, PDI (Figure 3a), and surface charge (Figure 3b) values of the BF and formulations containing the different emollients are shown in Figure 3. The results reveal that the smallest particle size (188 nm) is displayed by the BF since no emollients are included. On the other hand, the inclusion of cyclic structures like commercial silicones gave rise to higher particle size values (2726–3281 nm). The particle sizes of the formulations containing the new alternatives are comparable, except for sample BF+A1 (1671 nm). The particles' size of formulations prepared using commercial silicone alternatives is similar to that of samples containing the newly developed alternatives, except for sample BF+CS (2152 nm). The PDI value defines the particle size distribution in emulsions and can vary between 0 and 1.<sup>36</sup> The PDI values of our samples ranged from 0.148 to 0.469, demonstrating a small but acceptable level of homogeneity for these topical application samples. The particle surface charge (Figure 3b), defined as the zeta potential ( $\zeta$ ), is a stability characteristic that

determines the stability of the dispersion against aggregation or deposition.

Zeta potential values above  $\pm 30$  mV are considered moderately stable against aggregation because electrostatic repulsive forces are strong enough to prevent particles from aggregating.<sup>37,38</sup> The zeta potential values of the formulations remained generally constant in this study, ranging from  $-30.7$  to  $-39.4$  mV, demonstrating that all formulations were moderately stable.

The formulations' particle size was also calculated *in silico* (Table S1). Remarkably, MD simulations demonstrated that the molecules' superstructure evolved to what can be described as "round particles", indicating a micellar-like arrangement (not ordered, but in an entanglement), in agreement with experimental findings. In order to accommodate for simulation times, the systems simulated were narrowed down to the BF solely, plus BF+D5, BF+CC, BF+A2, BF+A3, BF+A5, and BF+A6, which gather successful and unsuccessful final formulations. The virtual systems were designed to keep the molecules in the same experimental environment and molecular proportion. However, on a nanometric scale, the number of molecules will be different than that found experimentally. Thus, the particle sizes inferred from both methods are not directly comparable, but a trend can be extrapolated. In fact, the BF resurfaces has the lowest size particle as should be expected, whereas BF+A2 has the highest particle size. BF+D5 display values different from experimentally available data; however, the other samples present particle sizes in accordance with the evaluation and are presented as shown in Figure 3a. An also noteworthy appointment from this analysis is the high viscosity of the samples. This component could explain the gap between computational and empirical data, as the latter could be influence the readings and interpret the particles as larger than they are. This is further supported by the relatively high PDI values presented in the aforementioned Figure 3a.

**3.2. Stability of Formulations at Different Temperatures over Time.** The investigation involved the evaluation of the organoleptic qualities of the formulations at various temperatures ( $-12$ ,  $4$  °C, room temperature, and  $37$  °C) over a period of 12 months. However, it should be noted that certain formulations demonstrate the occurrence of layer separation prior to the conclusion of the study.

The BF is the most stable (Table S2), as evidenced by the occurrence of separation during the centrifugation test only at months 11 and 12, after exposure at  $4$  °C, room temperature, and  $37$  °C. Regarding the other cosmetic formulations stored at  $4$  °C and room temperature, the occurrence of layer separation is observed after 6 months, except for BF+D5 and BF+D10, containing both commercial silicones. In addition, it should be noted that the critical temperatures for most formulations fall within are  $-12$  and  $37$  °C.

The pH of the formulations was evaluated once every month until the formulation underwent separation during the centrifugation test. Table S2 also presents the pH values at the time of manufacturing and after separation for each formulation. For all of the temperatures tested, there are no significant differences in the pH values between the initial state and the point at which the formulations become unstable.

**3.3. Stability of Formulations under Extreme Temperature Conditions.** Extreme temperature cycling tests can perceive instability faster than constant temperature storage. This test is not performed at a constant temperature because the goal is to simulate annual and daily temperature changes;

therefore, the test temperature varies cyclically over time. The cycle test was repeated three times. The samples were then examined for changes (pH, organoleptic characteristics, and layer separation—Table 4). The pH of all formulations slightly

**Table 4. Stability of the Cosmetic Formulations after Extreme Temperature Rest (pH, Organoleptic Characteristics, and Homogeneity)<sup>a</sup>**

	organoleptic properties after 3 cycles of extreme temperature testing					
	pH		color	Odor	appearance	layer separation after 3 cycles + centrifugation
	initial pH	final pH				
BF	4.983	5.075	N	N	H	no separation
BF+CP	4.871	5.123	N	N	H	no separation
BF+D5	4.940	5.161	N	N	H	no separation
BF+D10	4.829	5.175	N	N	H	no separation
BF+CC	4.934	5.107	N	N	H	no separation
BF+C5	4.924	5.087	N	N	H	no separation
BF+CS	4.891	5.085	N	N	H	no separation
BF+A1	4.916	5.043	N	N	S-	separation
BF+A2	4.805	5.115	N	N	S-	separation
BF+A3	4.996	5.040	N	N	S-	separation
BF+A4	4.898	5.093	N	N	H	separation
BF+A5	4.968	5.107	N	N	H	no separation
BF+A6	4.973	5.115	N	N	H	no separation

<sup>a</sup>H: homogeneous solution; S-: some surface separation (a small amount of transparent liquid forms on the surface); N: normal, similar to the control. BF: base formulation, BF+CP: base containing decamethylcyclopentasiloxane, BF+D5: base containing dimethicone 5 cst; BF+D10: base containing dimethicone 10 cst; BF+CC: base containing cetiol CC; BF+C5: base containing cetiol C5; BF+CS: base containing cetiol sensoft; BF+A1: base containing heptyl heptanoate; BF+A2: base containing heptyl octanoate; BF+A3: base containing heptyl decanoate; BF+A4: base containing decyl heptanoate; BF+A5: base containing decyl octanoate; BF+A6: base containing decyl decanoate.

increased from [4.8–4.9] to [5.0–5.1]. A macroscopic examination of the general appearance of the formulations was performed before centrifugation to assess the separation of the layers. After the cycle testing, the samples BF+CP, BF+D5, BF+D10, BF+CC, BF+C5, BF+CS, BF+A4, BF+A5, and BF+A6 showed a white color and homogeneity, whereas the samples BF+A1, BF+A2, and BF+A3 revealed some phase separation. When subjected to a centrifugation step at 3000 rpm for 30 min, these samples and the sample BF+A4 presented phase separation.

To understand the molecular distribution and differentiate the systems, explaining the phase separation phenomena, *in silico* density profiles along the simulation box were traced, throughout the simulation time (Figures 4 and 5). The spatial density profile assessment technique has already been described as a reliable approach to assess the systems' stability and to an extent, their spatial arrangement.<sup>23</sup> Typical RMSD analysis, usually employed to follow protein equilibration and structural stabilization, is not ideal for multicomponent mixtures, since the interaction among molecules will lead to large structural rearrangements. Thus, a density profile facilitates the perception of the formation of well-mixed formulations over time. Regarding systems' equilibration, note

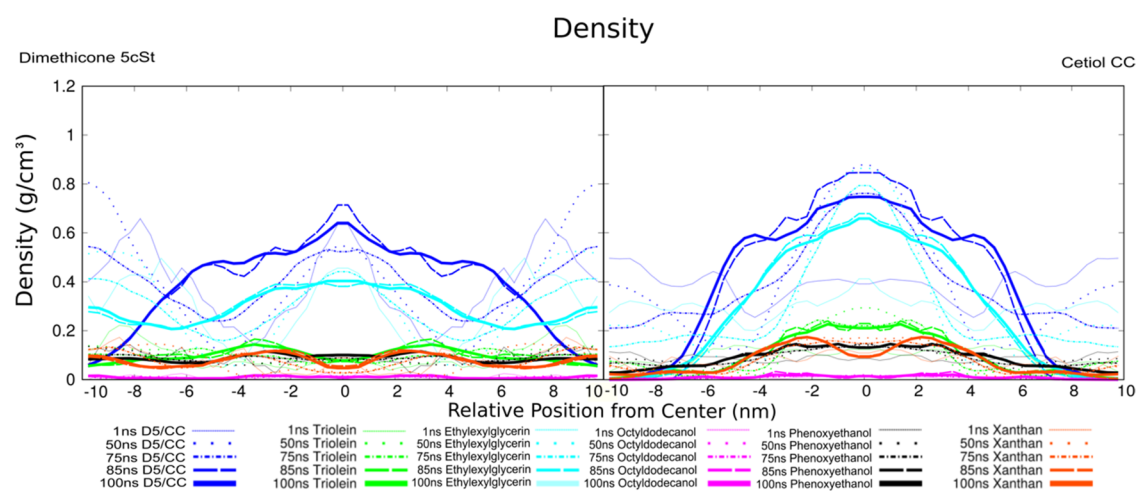


**Figure 4.** Density profiles—molecular distribution across simulation box extent—of formulations containing cetiol CC (right) and dimethicone at 5 cst (left).

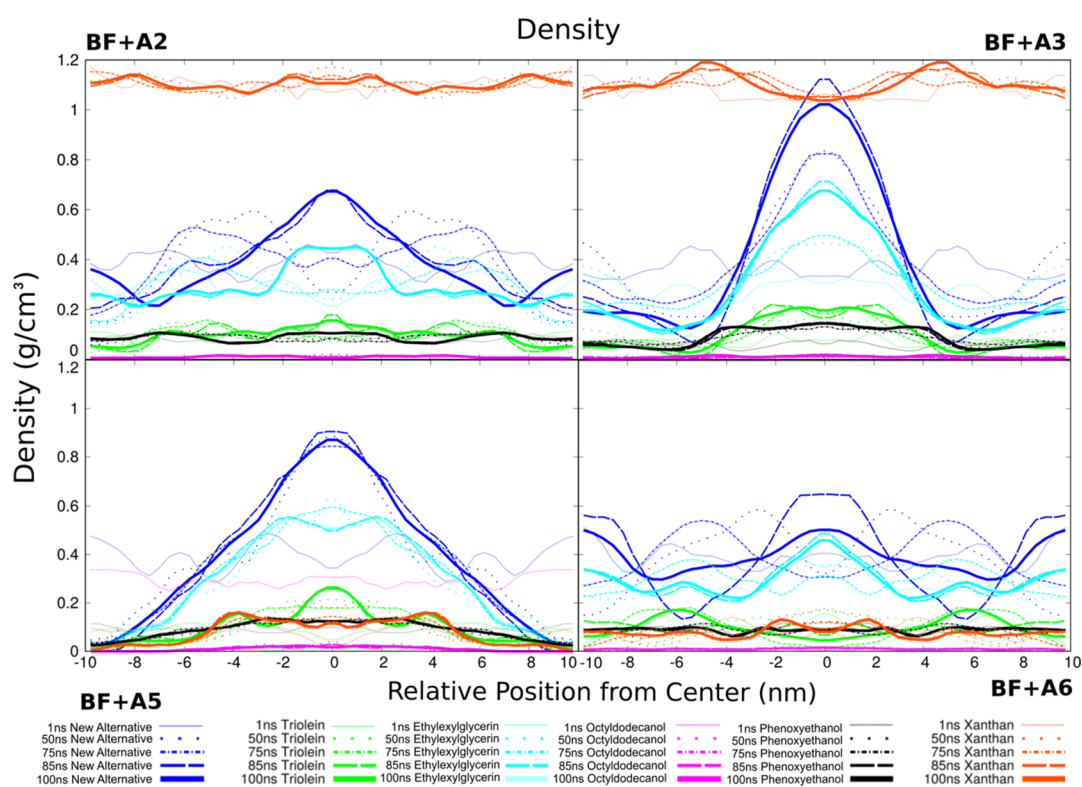


**Figure 5.** Density profiles across the simulation box of BF+A2, BF+A3 (top row, left and right, respectively); BF+A5 and BF+A6 (bottom row, left and right, respectively).

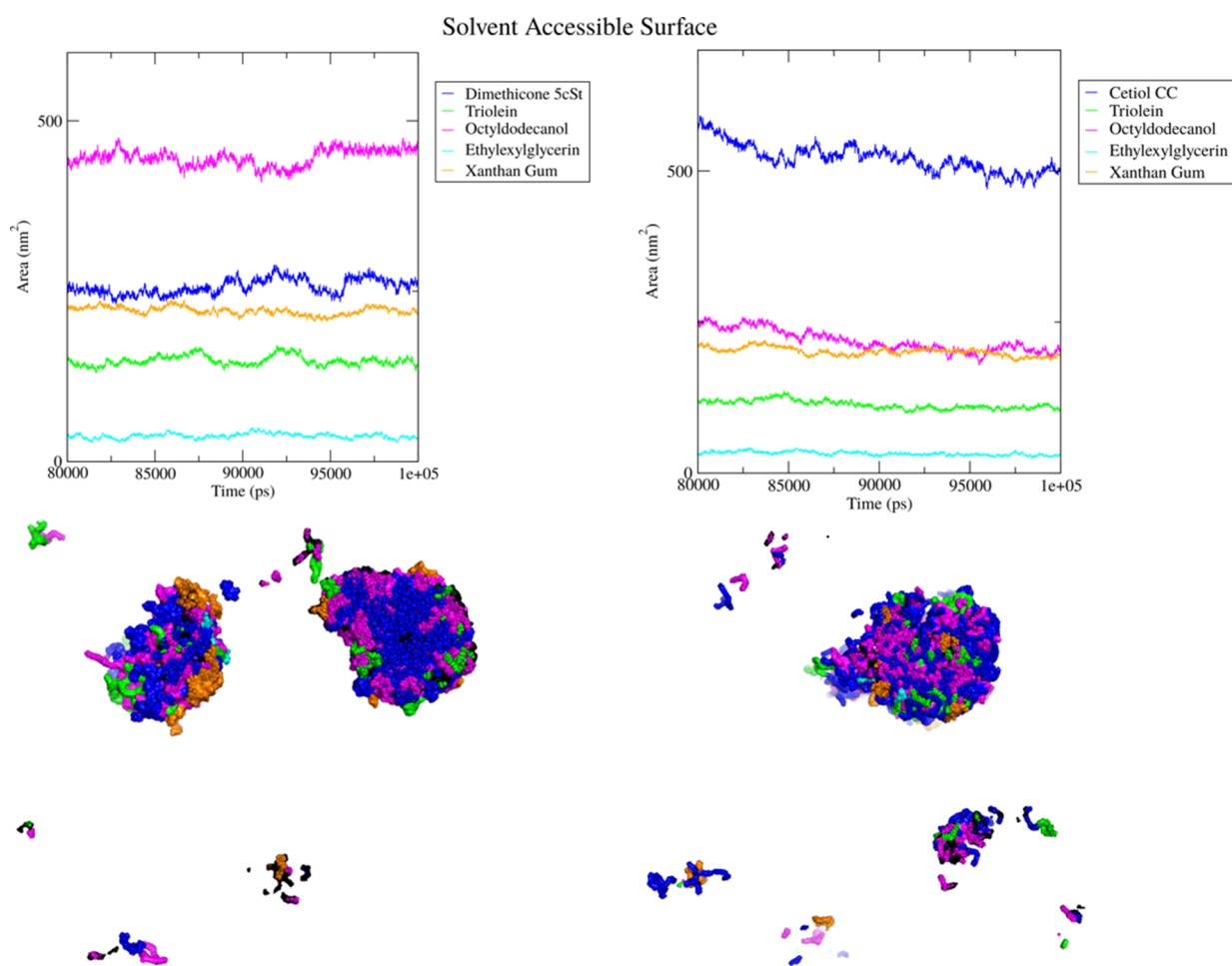
that most curves (Figures 4 and 5) are superimposed from 75 ns, and those where the peak does not coincide, differ by only 0.01–0.05 g/cm<sup>3</sup>, revealing equilibration by the end of the simulations.

Figure 4 displays the density profiles taken in different timesteps of simulation (1, 50, 75, 85, and 100 ns), which in turn will indicate how the components present in the emulsion distribute along their coordinates. While some variation is noted along the simulation, it is observable that for both BF+Cetiol and BF+Dimethicone 5 cst, the density profiles tend to get closer as time progresses. Again, while there is no clear juxtaposition of the density curves in the later stages of the simulation, the peak densities appear to be close to one

another, indicating stability. This is an expected result as complete stability of emulsion is hard to obtain in these types of solutions, and a similar pattern was observed when we previously tested a formulation containing commercial silicone alternatives.<sup>23</sup> In that work, most solutions were already stable at 100 ns in a self-assembly system, such as this one. The final conformation of these systems was also a micellar-like structure, as reported in that work.

Regarding the molecular distribution of compounds, both BF+D5 and BF+CC have similar profiles, organizing in a micellar fashion, with parabola-like curves, indicating a higher concentration of elements at a certain coordinate in the formulation. Other compounds organize in this parabolic





**Figure 6.** Spatial distribution analysis of the different components of the main aggregate. At the bottom is the most representative superstructure of both cetiol CC (right) and dimethicone at 5 cst (left), whereas at the top is the solvent-accessible surface of the same components. Molecules dispersed on the solvent phase are omitted (water, eutectic solvent, and phenoxyethanol).

curve, namely, ethylexyglycerin, and to a lesser extent, triolein and xanthan gum. Still on triolein, a recent study also addressed the partial density of this compound in several cosolvents, finding similar curves/propensity for this triglyceride by the end of the simulation.<sup>39</sup> In the case of phenoxyethanol and octyldodecanol, an almost linear curve is observed, which might indicate a higher degree of dispersion.

Data from Figure 5 indicate that all systems converge into a kind of parabola, representing the overall density profile of a micelle. Notoriously, BF+A5 and BF+A6 present a similar spatial distribution of molecules, with xanthan gum, octyldodecanol, phenoxyethanol, and triolein having a more dispersed profile into the aggregate, while the ethylexyglycerin and the ester demonstrated to be more concentrated in a region. In fact, these two silicone alternatives are the ones found to have similar behavior and properties to silicones, while BF+A2 and BF+A3 induce phase separation and thus present distinct density profiles.

Surprisingly, one similarity is found between BF+A2 and BF+A6, which present curves with noticeably lower amplitude and similar density profiles, whereas the opposite can be observed for BF+A3 and BF+A5, but further analysis must take place to understand these molecular distributions. Moreover, the more obvious particularity is the remarked different profile of xanthan in both BF+A2 and BF+A3, systems that induced separation. This might indicate that xanthan gum organizes

differently in the supramolecular structure and fails to stabilize it. In order to better assess the aforementioned, both clustering analysis and the molecular SASA were performed and discussed below.

The clustering analysis gives a visual perspective of the aggregates, revealing that the molecules of the ingredient Euxyl PE 90/10, used as a preservative, adopt different behaviors. The phenoxyethanol is dispersed along with the NADES (thus removed from cluster representation), serving as a solvent, while the ethylexyglycerin is part of the aggregate. This happens in all formulations regardless of the silicone/alternative used.

Comparing the silicone (dimethicone) and the commercial alternative (cetiol CC), through the SASA analysis, which gives a perspective of components' exposure to the solvents (and in what order the molecules are arranged, whether more in the interior or on the surface of the cluster), along with the most representative cluster groups, Figure 6 reveals a discrepancy between the distribution profiles of the silicone and cetiol, with the latter being more exposed. But one must consider that chemically, dimethicone, as a siloxane is quite different from an ester. In fact, the "blue" dimethicone in Figure 6 (left) appears to have its molecules more concentrated, protecting themselves from a hydrophobic effect, while the cetiol molecules are more dispersed (right).

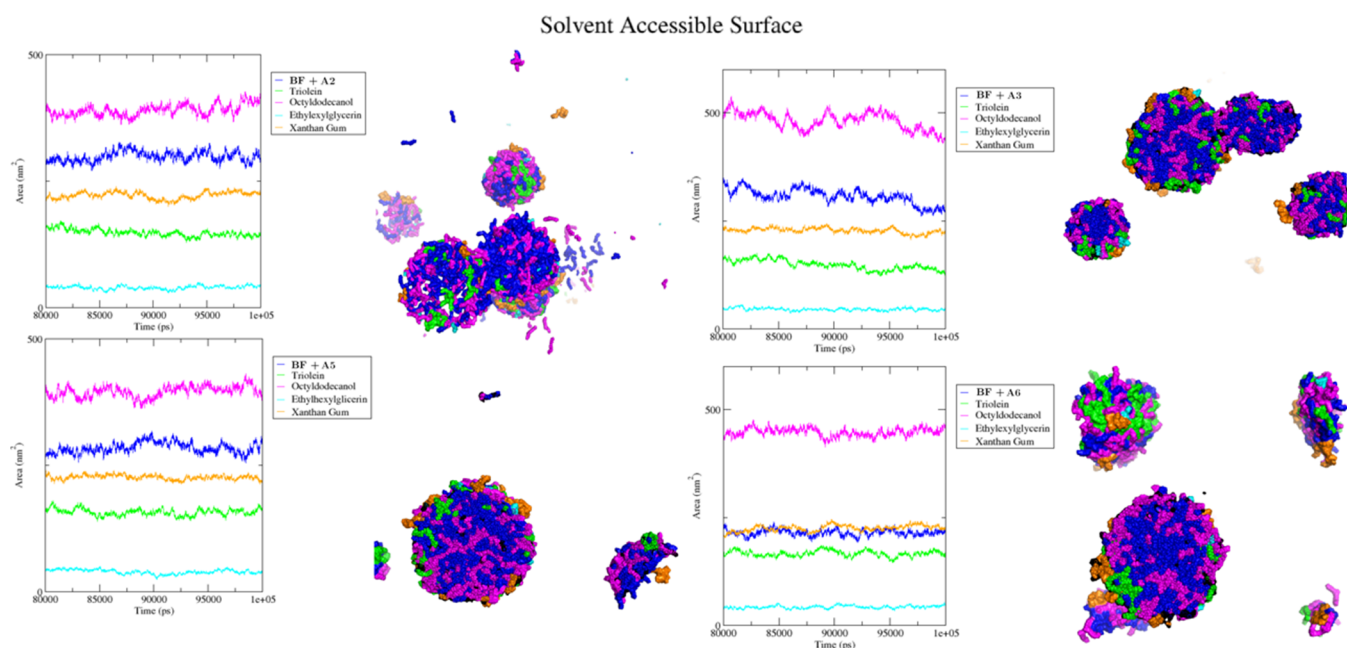


**Figure 7.** Spatial distribution analysis of the different components of the main aggregate. The SASA is presented on the left, while the illustration relative to the most representative cluster of that formulation is at the right of the graphs. Molecules dispersed on the solvent phase are omitted (water, eutectic solvent, and phenoxyethanol).

Importantly, the aggregate's superstructure containing dimethicone and cetiol CC is organized through the simulation box, in one or two micelles. These findings are thus expected to be found in similar products in order to mimic the properties found in these already available products.

Considering the density distribution of xanthan (Figure 5), unfortunately, the SASA analysis and the clustering visual inspection (Figure 7) cannot explain the distinct density profile of xanthan, as it appears to be exposed at the same rate and to be well-mixed with the other ingredients.

Regarding our new ester alternatives, even though the results presented in Figure 7 show a very similar distribution to the silicone itself through the SASA's analysis, a close visual inspection of the aggregates indicates a very different behavior of the molecules under study in the cases of BF+A2 (Heptyl Octanoate) and BF+A3 (Heptyl decanoate). These two were previously described to cause separation of the elements, and this behavior might be partly explained by their tendency for movement, as they produce undefined, broken superstructures in the case of BF+A2, or unstable, "semi-micelles" in the case of BF+A3. In contrast, both BF+A5 (Decyl octanoate) and BF+A6 (Decyl decanoate) systems present fewer aggregates and better-defined contents, much like the behavior of Dimethicone 5 cst in the same formulation. Another data to take note of is the almost juxtaposition of xanthan gum and BF+A6 in that area of the micelle. This is an interesting result that will require more analysis in order to discover if this is an advantageous behavior, as it is part of one of the better-behaving formulations.

**3.4. Stability of Formulations to Sunlight Exposure and Packaging.** In addition to physical and chemical analysis, it is critical to assess the cosmetic formulation's sensitivity to solar radiation. The formulations and packaging used may be sensitive to UV light, which, when combined with ambient oxygen, can cause product oxidation, resulting in the formation of free radicals. Numerous interactions take place between the

product, packaging, and external environment, such as the absorption of product elements by the container.

Following a 12-month period of examination, the majority of the cosmetic formulations studied herein exhibited consistent organoleptic characteristics, namely color, appearance, and odor, as observed during the initial assessment (Table 5). The

**Table 5.** Stability of the Cosmetic Formulations after 12 Months of Sunlight Exposure in Different Packaging<sup>a</sup>

formulations code	12 months exposure			
	glass	glass covered	plastic	plastic covered
BF	N	N	N	N
BF+CP	S	S	S-	S-
BF+D5	S-	S-	N	N
BF+D10	N	N	N	N
BF+CC	N	N	S-	N
BF+C5	N	N	N	N
BF+CS	N	N	N	N
BF+A1	N	N	N	N
BF+A2	S-	N	N	N
BF+A3	S	S	S	N
BF+A4	N	N	N	N
BF+A5	S-	N	N	N
BF+A6	N	N	N	N

<sup>a</sup>H: homogeneous solution; S: surface separation; S-: some surface separation (a small amount of transparent liquid forms on the surface); N: normal. BF: base formulation, BF+CP: base containing decamethylcyclopentasiloxane, BF+D5: base containing dimethicone 5 cst; BF+D10: base containing dimethicone 10 cst; BF+CC: base containing cetiol CC; BF+C5: base containing cetiol C5; BF+CS: base containing cetiol sensoft; BF+A1: base containing heptyl heptanoate; BF+A2: base containing heptyl octanoate; BF+A3: base containing heptyl decanoate; BF+A4: base containing decyl heptanoate; BF+A5: base containing decyl octanoate; BF+A6: base containing decyl decanoate.

formulation containing decamethylcyclopentasiloxane (CP) underwent separation in all tested conditions (glass, plastic, covered, and uncovered), demonstrating to be the least stable formulation to UV exposure and packaging type. Furthermore, sample BF+D5 exhibited minimal surface separation, limited to the glass packing material. Samples BF+A2 and BF+A5 experienced separation only within the uncovered glass packaging, while sample BF+A3 revealed separation for all the conditions tested, except for the uncovered plastic packaging. The results presented in this study reveal the impact of the container type on the stability of formulations to sunlight. The findings suggest that the stability of BF+CP, BF+D5, BF+A2, BF+A3, and BF+A5 compounds may have been compromised due to the interaction between solar exposure and packaging type.

**3.5. Texture Analysis.** Texture analysis is a tool that uses quantitative force measurements to convert them into qualitative organoleptic parameters. The interpretation of physical–mechanical parameters is a useful tool for obtaining relevant information about sensorial properties.<sup>6,18</sup> Texture analysis was carried out to physically evaluate the spreadability of the emulsions. Formulations intended for topical use application must have acceptable mechanical properties, namely ease of application and low firmness.<sup>1</sup>

**3.5.1. Spreadability.** The choice of an emollient can have a major impact on the ease of application of a cosmetic product. Higher emollient spreadability correlates with improved end-product usability.<sup>10</sup> Spreadability is a textural profile related to the feeling of touch when a product is applied to the skin, and it might influence product compliance.<sup>16,40</sup>

Figure 8 compares the work of shear values (%) of the formulations containing silicones, commercial alternatives, and new alternatives to the values of the BF (100%). These values are substantially associated with the formulation's spread-

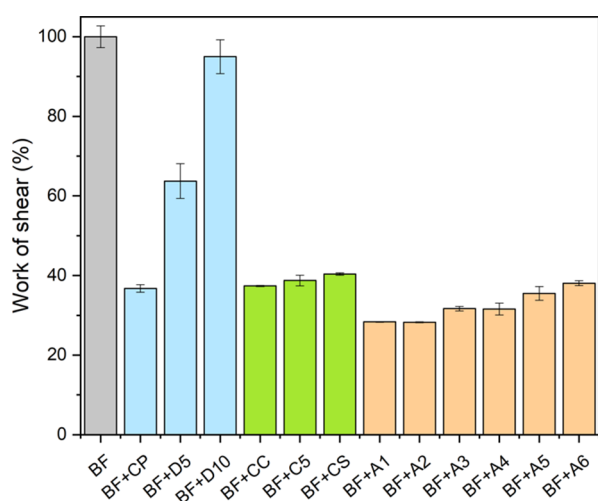


**Figure 8.** Work of shear (in relative percentages) of all cosmetic formulations. BF: base formulation, BF+CP: base containing decamethylcyclopentasiloxane, BF+D5: base containing dimethicone 5 cst; BF+D10: base containing dimethicone 10 cst; BF+CC: base containing cetiol CC; BF+C5: base containing cetiol C5; BF+CS: base containing cetiol sensoft; BF+A1: base containing heptyl heptanoate; BF+A2: base containing heptyl octanoate; BF+A3: base containing heptyl decanoate; BF+A4: base containing decyl heptanoate; BF+A5: base containing decyl octanoate; BF+A6: base containing decyl decanoate.

ability, supporting earlier research that shows these two features are inversely proportional, presenting a perfectly linear negative relationship.<sup>18</sup> Moreover, the lowest work of shear is reported to be related with the highest spreadability.<sup>38</sup>

Work of shear values differed significantly between the BF (no silicone or alternatives) and the same BF containing a silicone/alternative. The spreadability of the emulsions BF+D5 and BF+D10 (commercial silicones) is lower than that of all other emulsions (work of shear: 64 and 95%, respectively), whereas samples BF+D10 have the lowest spreadability because of the high viscosity (10 cst). The formulations containing the new alternatives (BF+A1 to BF+A6) are easy to spread, with work of shear values (28–38%) that outperform the commercial alternatives (BF+CC, BF+C5, and BF+CS).

Considering the *in silico* diffusivity analysis presented in Section 3.1, the new silicone alternatives also proved to move faster within the formulation than BF+D5 or BF+CC. This might indicate that they respond easily to traction and mechanical stress forces agreeing with what was presented in Figure 8 and is discussed above regarding the work of shear.

**3.5.2. Back Extrusion Test.** Back extrusion tests involve applying force to a material until it flows (compression). The maximum force required for material extrusion is used as a quality indicator to predict sensory characteristics.<sup>16,17</sup> The sample has a large contact area with the back-extrusion test, and the firmness (the maximum force that the sample exerts on the probe during penetration), consistency (the total work performed by the probe to penetrate the sample to a defined depth), cohesiveness (the maximum absolute force measured during probe withdrawal), and the index of viscosity are the main parameters evaluated. This test is carried out on almost the entire sample in the container and allows for the simulation of different forms of cosmetic cream handling, such as mild or intense (equivalent to gentle finger dipping or extrusion of a considerable amount of sample). BF (base formulation/control) shows high values of firmness (maximum of the positive curve) and consistency (area under the positive curve) followed by BF+D10 and BF+D5 (Figure 9). The cohesiveness and viscosity index values follow the same pattern as the other two properties, with BF and BF+D10 displaying the highest modulus values. These findings suggest that the emollients dimethicone 5 cst and dimethicone 10 cst (BF+D5 and BF+D10) may increase the system stability because formulations with greater consistency and viscosity index impose resistance to the movement of the emulsion's internal phase and avoid stability loss.<sup>16</sup>

The formulations containing the new alternatives present firmness, consistency, cohesiveness, and viscosity index values lower than those of formulations containing the silicones and the commercial alternatives. These values suggest excellent spreadability, demonstrating their great emollient capacity, in comparison to the commercial compounds.

**3.6. Contact Angle of Formulations with a Solid Surface.** Contact angle measurements were performed only for the base formulation (BF, control), one formulation containing a commercial silicone (BF+D5), one formulation containing a commercial alternative (BF+CC), and one formulation containing one of the new alternatives produced (BF+A6). To facilitate the interpretation of the data, a single sample was chosen from each category (silicones, commercial alternatives, and new alternatives) to be included in the study.

Contact angle measurements for BF and formulations containing silicones/alternatives (BF+D5, BF+CC and BF

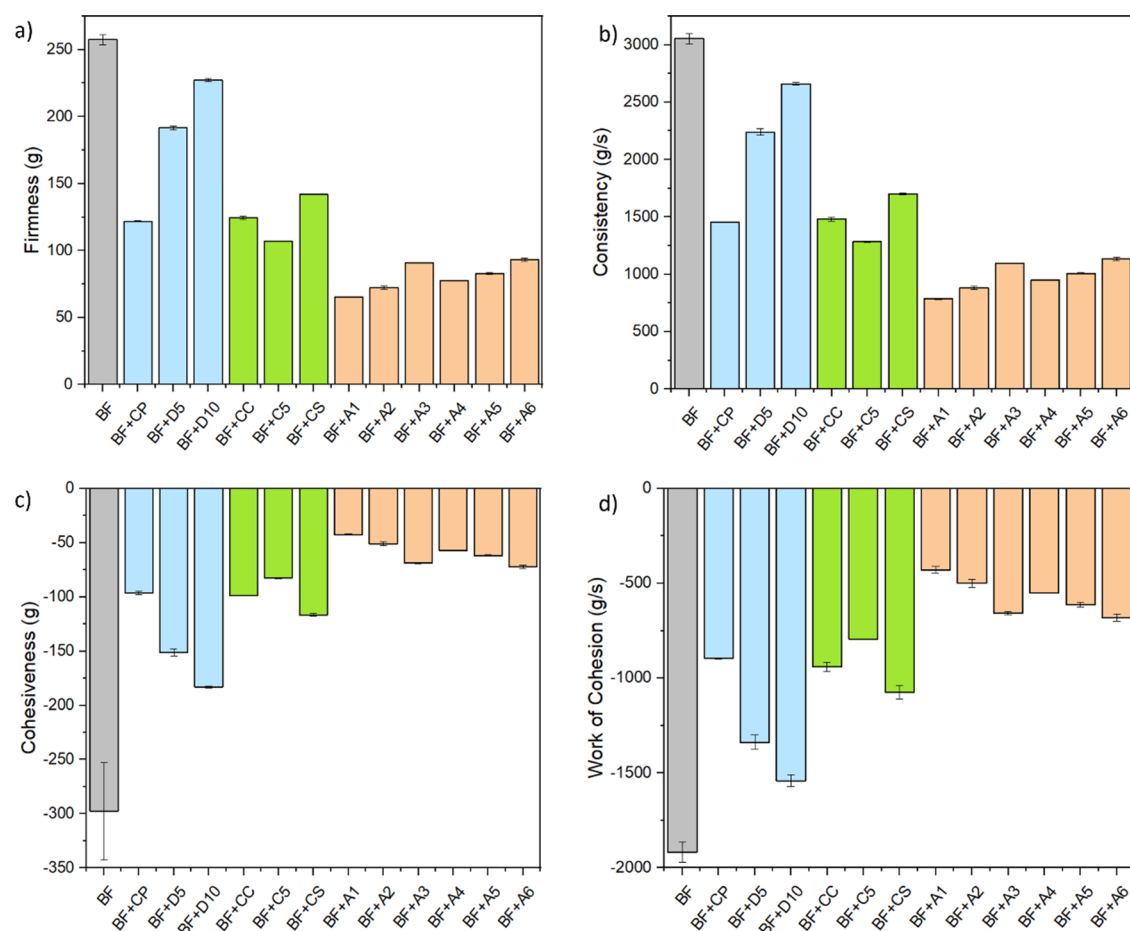


**Figure 9.** Textural Parameters of the Cosmetic Emulsions at Room Temperature Firmness (a), Consistency (b), cohesiveness (c), and viscosity index (d) were taken from a back-extrusion test. Results are the average of duplicate samples, and bars represent standard. BF: base formulation, BF+CP: base containing decamethylcyclopentasiloxane, BF+D5: base containing dimethicone 5 cst; BF+D10: base containing dimethicone 10 cst; BF+CC: base containing cetiol CC; BF+C5: base containing cetiol C5; BF+CS: base containing cetiol sensoft; BF+A1: base containing heptyl heptanoate; BF+A2: base containing heptyl octanoate; BF+A3: base containing heptyl decanoate; BF+A4: base containing decyl heptanoate; BF+A5: base containing decyl octanoate; BF+A6: base containing decyl decanoate.

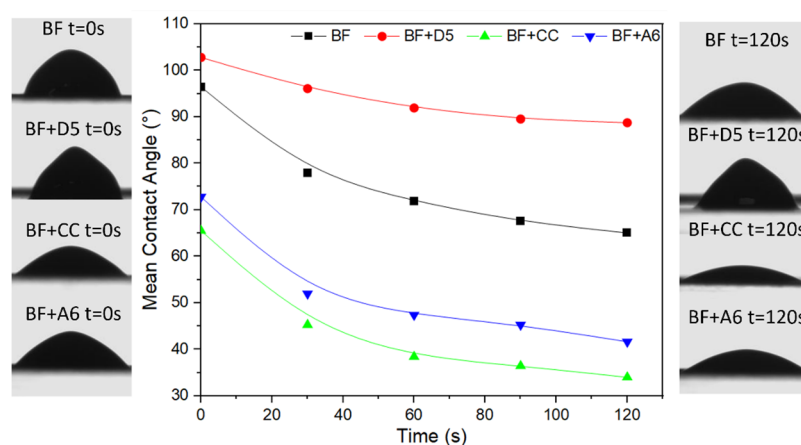


**Figure 10.** Contact angle evolution of cosmetic formulations deposited on the PMMA surface. BF: base formulation, BF+D5: base containing dimethicone 5 cst; BF+CC: base containing cetiol CC; BF+A6: base containing decyl decanoate.

+A6) were performed from the initial time, as the drop of liquid was deposited on the PMMA surface (considered 0s) until it reached a measurable constant value (120s) (Figure 10). At the  $t = 0$  s, the initial values are  $96.5^\circ$  for the BF,  $102.8^\circ$  for the formulation containing dimethicone 5 cst,  $65.5^\circ$  for

formulation containing cetiol CC (BF+CC), and  $72.8^\circ$  for the formulation containing the new alternative A6 (BF+A6). Observing Figure 10, the formulation containing the commercial silicone (BF+D5) reveals the highest initial contact angle followed by the BF without any emollient

added. The contact angle value is inversely proportional to the spreadability of the product on the surface of PMMA.<sup>6</sup> Therefore, these two samples exhibit much lower spreadability compared with the other formulations that contain alternative emollients. Over time, the formulation containing D5 exhibits reduced spreadability, with a slightly lower contact angle (88.8°) after 120 s. Moreover, the formulations containing alternatives to silicones (commercial or news), BF+CC and BF+A6, changed from contact angles of 65.5° and 72.8° to 34° and 41.7°, respectively. The curves of contact angle versus time of formulations BF+CC and BF+A6 exhibit a rapid exponential decrease, corresponding to the spontaneous spreading of each formulation on the solid support.

These contact angle measurements appear to be crucial for anticipating the spreadability of cosmetic formulations, and it is possible to estimate the spreading ability of various silicones and alternatives using an objective method rather than a sensory evaluation. Furthermore, the contact angle measurements were taken with a PMMA surface, which is a fairly reproducible, easy-to-use, and low-cost material when compared to real and synthetic skin.<sup>6</sup>

**3.7. Rheological Analysis.** The rheological characterization of a cosmetic emulsion allows for the measurement of essential aspects related with the chemical composition of the formulations as well as its impact on consumer perception.<sup>16</sup> Rheology is the science of flow and deformation of materials by shear rates and shear stress. The spreadability of cosmetics products is influenced by their flow behavior. For the rheology testing, only four samples were tested: a formulation containing commercial silicone (BF+D5), a formulation containing a commercial silicone alternative (BF+CC), a formulation containing a new alternative (BF+A6), and a BF with no incorporated emollient incorporated (BF).

**3.7.1. Viscosity: Shear Flow Test.** The viscosity as a function of shearing rate provides important information about the processing and performance of a certain material. This is useful in the development process, where a product is subjected to a variety of shear rates during stirring, dispensing, and pumping.

A controlled rheological analysis was carried out to investigate the viscosity trend as a function of the shear rate. Figure 11 shows that all formulations exhibit a classical shear thinning behavior (pseudoplastic), with viscosity decreasing progressively under shear application.<sup>41</sup> This is a crucial attribute for cosmetic creams because when applied to the skin (by shearing force provided by hand), the viscosity drops, and the spreadability is predicted to improve. The viscosity value used for comparison is the initial shear rate value (0–2 s<sup>-1</sup>) because, after a certain value (4 s<sup>-1</sup>), the behavior of the samples is maintained and the viscosity is very low.

The control formulation (BF) has, as expected, higher viscosity at a low shear rate than the samples containing silicones/alternatives since these compounds are expected to improve the spreadability of the cosmetics formulations. The silicone formulation (BF+D5) has the highest viscosity after BF; however, the formulation containing the new alternative (BF+A6) has a viscosity equivalent to that of the commercial silicone formulation (BF+D5), indicating that the new alternative (BF+A6) possesses emollient qualities.

In silico studies of viscosity did not result in meaningful values for these complex simulations. In fact, as stated in our previous work, although the energy module in GROMACS (used to evaluate the viscosity) has been optimized over the

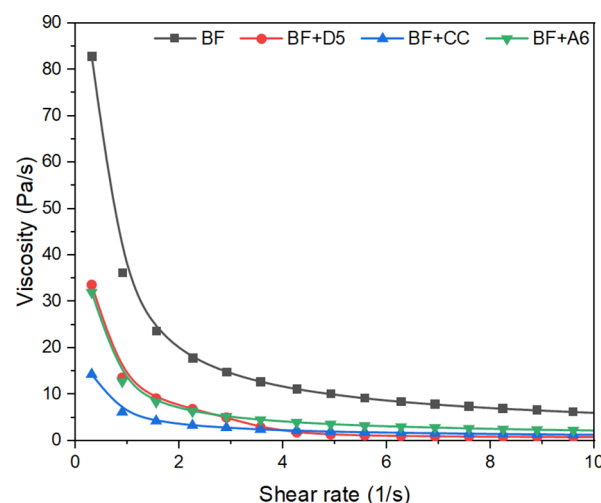


**Figure 11.** Viscosity trend as a function of the shear rate values of BF, formulation containing dimethicone 5 cst (BF+D5), formulation containing cetiol CC (BF+CC), and formulation containing a new alternative, decyl decanoate (BF+A6).

years, this tool must be improved to reproduce with better accuracy the experimental results.<sup>23,42</sup>

**3.7.2. Oscillation Amplitude Sweep Test: Determination of the Linear-Viscoelastic Region.** Oscillation amplitude sweep measurements enabled the LVR, where stress and strain are proportional. The applied stresses in the LVR are insufficient to produce a structural breakdown, and hence, microstructural characteristics are being determined. The LVR can be determined by running a stress or strain sweep test and watching the point on the graph where  $G'$  and  $G''$  overlap. The end of the linear-viscoelastic range is reached at oscillation strain values, where the rheological parameters will start to change from constant behavior. Solid materials exhibit elastic behavior, whereas fluid materials exhibit viscous behavior. Viscoelastic/pseudoplastic materials, such as emulsions/cosmetics, are neither true fluids nor solids but exhibit both elastic and viscous behavior—a storage/elastic component represented by  $G'$  and a loss/viscous component represented by  $G''$ .<sup>20,43,44</sup>

The critical strain used in this case was 4%; below this value, the structure is intact, the formulation behaves solid-like, and  $G' > G''$ , indicating that the cosmetic formulation is highly structured. Increasing the strain above the critical strain causes the network structure to be disrupted (Figure 12) and the material becomes progressively more fluid-like, the storage modulus declines and  $G''$  exceeds  $G'$ . Figure 12 shows that the formulation containing the new alternative (BF+A6) becomes more fluid ( $G''$  exceeds  $G'$ ) at a smaller oscillation strain than the formulations containing silicone (BF+D5) or commercial alternative (BF+CC). This demonstrates that BF+A6 has an emollient function that resulted in a more fluidic formulation and thus a smoother formulation than silicones and commercial alternatives.

**3.7.3. Frequency Sweep Test.** After the fluid's LVR has been defined by a strain sweep, the viscoelastic property as a function of the frequency was investigated using the frequency sweep test, which was conducted at a fixed oscillation amplitude (4%) within the linear viscoelastic range. Figure 13 shows that all cosmetics formulations have  $G' > G''$ , indicating that the system's elastic components dominated the viscous components and that the system's structure was held

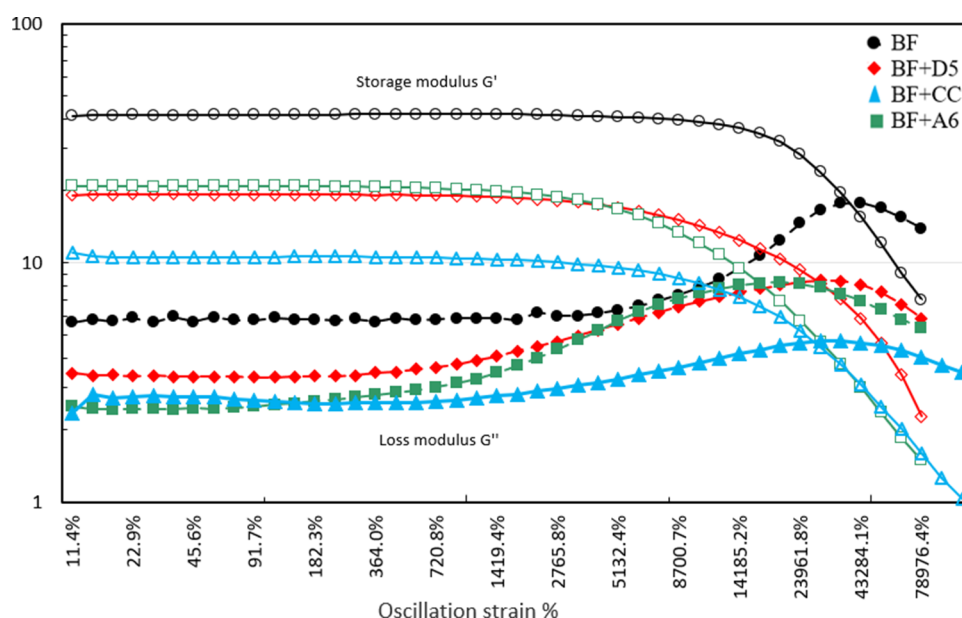


**Figure 12.** Strain sweep of BF, formulation with dimethicone 5 cst (BF+D5), formulation with cetiol CC (BF+CC) and formulation with new alternative decyl decanoate (BF+A6).  $G'$  represents the not filled symbols, and  $G''$  represents the filled symbols.

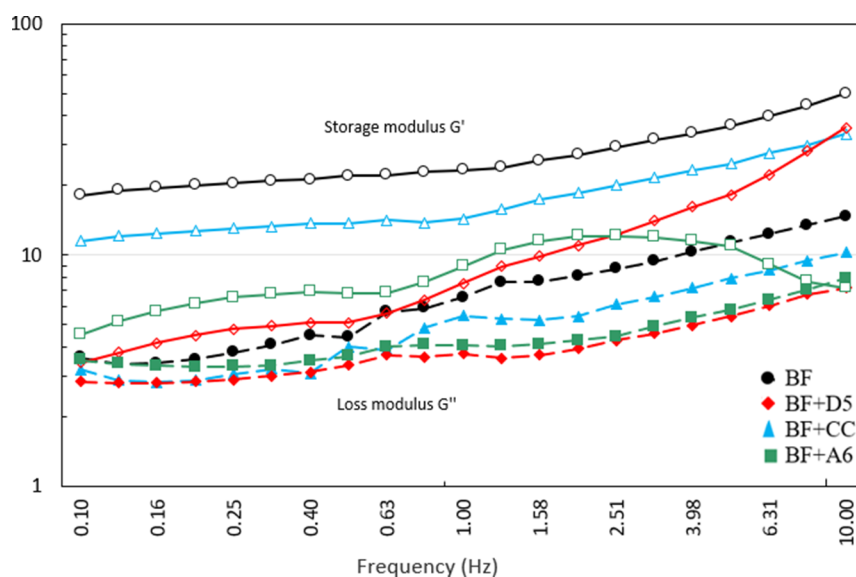


**Figure 13.** Frequency sweep of BF, formulation containing dimethicone 5 cst (BF+D5), formulation containing cetiol CC (BF+CC), and formulation containing the new alternative decyl decanoate (BF+A6).  $G'$  represents the not filled symbols, and  $G''$  represents the filled symbols.

together by physical bonds between the macromolecules.<sup>4</sup> The BFs had the highest  $G'$  values, which correspond to the highest viscosity values in the flow curves, demonstrating the role of emollients and microstructure on system rheology. The sample BF+A6 has the lowest  $G'$  and  $G''$  values, demonstrating that decyl decanoate ester has a high emollient capacity when compared to other commercial emollients (BF+D5 and BF+CC).

#### 4. CONCLUSIONS

The goal of this work was to find new silicone alternatives based on ester-based compounds. For this, the innovative ester-based compounds, previously synthesized, were incorporated into a BF, to replace commercial silicone-based compounds. The findings from both experimental and computational analyses indicate that long-chain esters,

particularly those with a “decyl” structure, are the most favorable choices to be included in cosmetic compositions. During the experimental conditions, it was noted that the newly generated alternatives demonstrated stability for a duration of 6 months when stored at both 4 °C and room temperature. Throughout this period, the pH of the formulations remained consistent, and there were no discernible changes in the sensory features, such as color, look, and odor. The spreadability, which is the primary function of an emollient, of the newly developed ester-based alternatives is similar to that of existing commercial alternatives (BF+CC, BF+CS, and BF+CS), but it is notably superior to that of the tested commercial silicones BF+CP, BF+D5, and BF+D10. The validation of this outcome has been proven through the execution of various experiments, such as texturometer analysis, rheological analysis, and contact angle

measurement. Computationally, all systems have converged to somewhat stable superstructures, with the ester-based alternatives performing slightly better with more cohesive structures and fewer cluster groups, in the case of A5 and A6, aligned with previous findings. Furthermore, all of the other options exhibit comparable interactions with the solvent. However, A6 displays a nearly identical exposed surface area to the solvent as xanthan gum, which is a recognized agent for binding and stabilizing emulsions. This factor may contribute to A6's superior overall stability.

Molecular modeling is also evolving to optimize protocols, methods, and analysis to follow this type of system, further understanding the molecular processes behind emulsion formation, molecular aggregation, and stability. This will allow the optimization of industrial processes as well as the creation of new and more efficient strategies for R&D projects, reducing resource-heavy and costly tasks and thus bettering the companies' ecological footprint and finances.

Ultimately, in light of the growing cosmetics industry, innovative solutions have emerged through advancements in modern science and technology. There are methods available to duplicate and enhance the characteristics found in conventional cosmetics, and this endeavor adds to the progress of contemporary cosmetics with an environmentally friendly alternative. The techniques employed in this study illustrate the benefits of combining traditional methods with modern *in silico* approaches to obtain these products. This approach not only facilitates the development of similar products but also enables further advancements in related research. These findings have implications not only for skincare but also for all sectors of the cosmetics industry, potentially leading to the establishment of an environmentally sustainable industry.

## ■ ASSOCIATED CONTENT

### SI Supporting Information

The Supporting Information is available free of charge at <https://pubs.acs.org/doi/10.1021/acs.iecr.4c00886>.

Aggregates' particle size (Table S1) and organoleptic properties (pH, phase separation) evaluated at different temperatures over time (Table S2) (PDF)

## ■ AUTHOR INFORMATION

### Corresponding Author

Tarsila G. Castro – CEB – Center of Biological Engineering, University of Minho, 4710-057 Braga, Portugal; [orcid.org/0000-0002-1040-459X](https://orcid.org/0000-0002-1040-459X); Email: [castro.tarsila@ceb.uminho.pt](mailto:castro.tarsila@ceb.uminho.pt)

### Authors

Tiago Ferreira – CEB – Center of Biological Engineering, University of Minho, 4710-057 Braga, Portugal; SOLFARCOS – Soluções Farmacêuticas e Cosméticas, Lda., 4700-034 Braga, Portugal; [orcid.org/0000-0003-3182-7935](https://orcid.org/0000-0003-3182-7935)

Diana Rocha – CEB – Center of Biological Engineering, University of Minho, 4710-057 Braga, Portugal; SOLFARCOS – Soluções Farmacêuticas e Cosméticas, Lda., 4700-034 Braga, Portugal

David Freitas – CEB – Center of Biological Engineering, University of Minho, 4710-057 Braga, Portugal

Jennifer Noro – CEB – Center of Biological Engineering, University of Minho, 4710-057 Braga, Portugal

SOLFARCOS – Soluções Farmacêuticas e Cosméticas, Lda., 4700-034 Braga, Portugal

Mariana de Castro – CEB – Center of Biological Engineering, University of Minho, 4710-057 Braga, Portugal; SOLFARCOS – Soluções Farmacêuticas e Cosméticas, Lda., 4700-034 Braga, Portugal

Catarina Roque – CEB – Center of Biological Engineering, University of Minho, 4710-057 Braga, Portugal; SOLFARCOS – Soluções Farmacêuticas e Cosméticas, Lda., 4700-034 Braga, Portugal

Diana Guimarães – CEB – Center of Biological Engineering, University of Minho, 4710-057 Braga, Portugal; SOLFARCOS – Soluções Farmacêuticas e Cosméticas, Lda., 4700-034 Braga, Portugal

Ana Loureiro – CEB – Center of Biological Engineering, University of Minho, 4710-057 Braga, Portugal; SOLFARCOS – Soluções Farmacêuticas e Cosméticas, Lda., 4700-034 Braga, Portugal

Carla Silva – CEB – Center of Biological Engineering and LABBELS – Associate Laboratory in Biotechnology and Bioengineering and Microelectromechanical Systems, University of Minho, 4710-057 Braga, Portugal

Artur Cavaco-Paulo – CEB – Center of Biological Engineering and LABBELS – Associate Laboratory in Biotechnology and Bioengineering and Microelectromechanical Systems, University of Minho, 4710-057 Braga, Portugal; SOLFARCOS – Soluções Farmacêuticas e Cosméticas, Lda., 4700-034 Braga, Portugal; [orcid.org/0000-0001-7204-2064](https://orcid.org/0000-0001-7204-2064)

Complete contact information is available at: <https://pubs.acs.org/10.1021/acs.iecr.4c00886>

### Author Contributions

Both authors contributed equally to this work.

### Funding

All authors thank FCT under the scope of the strategic funding of UIDB/04469/2020 unit, and by LABBELS—Associate Laboratory in Biotechnology, Bioengineering, and Microelectromechanical Systems, LA/P/0029/2020. Rocha (2022.13494. BDANA) and Freitas (SFRH/BD/147190/2019) thanks the financial support from the Portuguese Foundation for Science and Technology (FCT).

### Notes

The authors declare the following competing financial interest(s): Artur Cavaco-Paulo is a Professor at the University of Minho (UM) and the co-founder of SOLFARCOS, a spin-off company of the UM, where he holds the position of CSO. Loureiro and Guimaraes are researchers employed by SOLFARCOS and collaborators of CEB-UM. Noro was a researcher at SOLFARCOS during work development. Ferreira is a PhD student of the Doctoral Program in Chemical and Biological Engineering developing his work at the Centre of Biological Engineering of the UM and being supported by SOLFARCOS with a PhD grant. Rocha is a PhD student of the Doctoral Program in Chemical and Biological Engineering developing her work at the Centre of Biological Engineering of the UM and being supported, during the work development, by SOLFARCOS with a PhD grant. Castro, Freitas and Silva declare no competing interests.

## ACKNOWLEDGMENTS

Ferreira and Castro thank the funding and computational infrastructure provided by SOLFARCOS (Soluções Farmacêuticas e Cosméticas, Lda.) and the Department of Informatics of University of Minho: this research was developed with the support of computing facilities provided by the Project: “Search-ON2: Revitalization of HPC infrastructure of UMinho” (NORTE-07-0162-FEDER-000086), cofunded by the North Portugal Regional Operational Programme (ON.2 – O Novo Norte), under the National Strategic Reference Framework (NSRF), through the European Regional Development Fund (ERDF). Castro acknowledges FCT and Oblivion HPC for the project 2022.15868.CPCA.A1 which granted additional computational infrastructure for this study.

## REFERENCES

- (1) Estanqueiro, M.; Conceição, J.; Amaral, M. H.; Sousa Lobo, J. M. Characterization, Sensorial Evaluation and Moisturizing Efficacy of Nanolipidgel Formulations. *Int. J. Cosmet. Sci.* **2014**, *36* (2), 159–166.
- (2) Loo, C. H.; Basri, M.; Ismail, R.; Lau, H. L. N.; Tejo, B. A.; Kanthimathi, M. S.; Hassan, H. A.; Choo, Y. M. Effect of Compositions in Nanostructured Lipid Carriers (NLC) on Skin Hydration and Occlusion. *IJN* **2012**, *8* (1), 13–22.
- (3) Gore, E.; Picard, C.; Savary, G. Spreading Behavior of Cosmetic Emulsions: Impact of the Oil Phase. *Biotribology* **2018**, *16*, 17–24.
- (4) Dederen, J. C.; Chavan, B.; Rawlings, A. V. Emollients Are More than Sensory Ingredients: The Case of Isostearyl Isostearate. *International Journal of Cosmetic Science* **2012**, *34* (6), 502–510.
- (5) Nacht, S.; Close, J.-A.; Yeung, D.; Gans, E. H. Skin Friction Coefficient: Changes Induced by Skin Hydration and Emollient Application and Correlation with Perceived Skin Feel. *J. Soc. Cosmet. Chem.* **1981**, *32*, 55–65.
- (6) Savary, G.; Grisel, M.; Picard, C. Impact of Emollients on the Spreading Properties of Cosmetic Products: A Combined Sensory and Instrumental Characterization. *Colloids Surf., B* **2013**, *102*, 371–378.
- (7) Gorcea, M.; Laura, D. Evaluating the Physicochemical Properties of Emollient Esters for Cosmetic Use. *Cosmetics & Toiletries*. <https://www.cosmeticsandtoiletries.com/testing/sensory/article/21836556/evaluating-the-physicochemical-properties-of-emollient-esters-for-cosmetic-use> (accessed 2023–09–04).
- (8) Douguet, M.; Picard, C.; Savary, G.; Merlaud, F.; Loubatbouleuc, N.; Grisel, M. Spreading Properties of Cosmetic Emollients: Use of Synthetic Skin Surface to Elucidate Structural Effect. *Colloids Surf., B* **2017**, *154*, 307–314.
- (9) Goussard, V.; Aubry, J.-M.; Nardello-Rataj, V. Bio-Based Alternatives to Volatile Silicones: Relationships between Chemical Structure, Physicochemical Properties and Functional Performances. *Adv. Colloid Interface Sci.* **2022**, *304*, No. 102679.
- (10) Littich, R.; Ilseman, A.; Hategan, G.; Liang, Y.; Koers, K.; Morie-Bebel, M. *Bio-based alternatives for silicone and petrochemical emollients from natural oil metathesis - tks | publisher, event organiser, media agency.* HPC today | TKS Publisher. [https://www.teknoscience.com/tks\\_article/bio-based-alternatives-for-silicone-and-petrochemical-emollients-from-natural-oil-metathesis/](https://www.teknoscience.com/tks_article/bio-based-alternatives-for-silicone-and-petrochemical-emollients-from-natural-oil-metathesis/) (accessed 2023–09–04).
- (11) Cornwell, P. A. A Review of Shampoo Surfactant Technology: Consumer Benefits, Raw Materials and Recent Developments. *International Journal of Cosmetic Science* **2018**, *40* (1), 16–30.
- (12) Badmus, S. O.; Amusa, H. K.; Oyehan, T. A.; Saleh, T. A. Environmental Risks and Toxicity of Surfactants: Overview of Analysis, Assessment, and Remediation Techniques. *Environ. Sci. Pollut. Res.* **2021**, *28* (44), 62085–62104.
- (13) Roque, C. S.; de Castro, M.; Castro, T. G.; Silva, C.; Cavaco-Paulo, A.; Noro, J. Solvent-Free Synthesis of Hydrophobic and Amphiphilic Esters Using a Chemically Modified Lipase from *Thermomyces Lanuginosus*: A Comparative Study with Native and Immobilized Forms. *ChemBioChem.* **2024**, *25* (4), No. e202300843.
- (14) Anzali, S.; Pflücker, F.; Heider, L.; Jonczyk, A. Computational Approaches to Cosmetics Products Discovery. In *Applied Chemoinformatics*; John Wiley & Sons, Ltd, 2018; pp 527–546. DOI: DOI: 10.1002/9783527806539.ch11.
- (15) Carpio, L. E.; Sanz, Y.; Gozalbes, R.; Barigye, S. J. Computational Strategies for the Discovery of Biological Functions of Health Foods, Nutraceuticals and Cosmeceuticals: A Review. *Mol. Divers* **2021**, *25* (3), 1425–1438.
- (16) César, F. C. S.; Maia Campos, P. M. B. G. Influence of Vegetable Oils in the Rheology, Texture Profile and Sensory Properties of Cosmetic Formulations Based on Organogel. *International Journal of Cosmetic Science* **2020**, *42* (5), 494–500.
- (17) Calixto, L. S.; Infante, V. H. P.; Maia Campos, P. M. B. G. Design and Characterization of Topical Formulations: Correlations Between Instrumental and Sensorial Measurements. *AAPS PharmSci-Tech* **2018**, *19* (4), 1512–1519.
- (18) Calixto, L. S.; Maia Campos, P. M. B. G. Physical–Mechanical Characterization of Cosmetic Formulations and Correlation between Instrumental Measurements and Sensorial Properties. *International Journal of Cosmetic Science* **2017**, *39* (5), 527–534.
- (19) Tafuro, G.; Costantini, A.; Baratto, G.; Francescato, S.; Busata, L.; Semenzato, A. Characterization of Polysaccharidic Associations for Cosmetic Use: Rheology and Texture Analysis. *Cosmetics* **2021**, *8* (3), 62.
- (20) Martins, D.; Rocha, C.; Dourado, F.; Gama, M. Bacterial Cellulose-Carboxymethyl Cellulose (BC:CMC) Dry Formulation as Stabilizer and Texturizing Agent for Surfactant-Free Cosmetic Formulations. *Colloids Surf., A* **2021**, *617*, No. 126380.
- (21) MarvinSketch 17.16 from ChemAxon Ltd. <https://chemaxon.com/marvin>; january 2023.
- (22) Dodda, L. S.; Cabeza de Vaca, I.; Tirado-Rives, J.; Jorgensen, W. L. LigParGen Web Server: An Automatic OPLS-AA Parameter Generator for Organic Ligands. *Nucleic Acids Res.* **2017**, *45* (W1), W331–W336.
- (23) Ferreira, T.; Loureiro, A.; Noro, J.; Cavaco-Paulo, A.; Castro, T. G. Addressing the Structural Organization of Silicone Alternatives in Formulations by Molecular Dynamics Simulations and a Novel Equilibration Protocol. *Polymers* **2023**, *15* (4), 796.
- (24) Bussi, G.; Donadio, D.; Parrinello, M. Canonical Sampling through Velocity Rescaling. *J. Chem. Phys.* **2007**, *126* (1), No. 014101.
- (25) Bussi, G.; Zykova-Timan, T.; Parrinello, M. Isothermal-Isobaric Molecular Dynamics Using Stochastic Velocity Rescaling. *J. Chem. Phys.* **2009**, *130* (7), No. 074101.
- (26) Martoňák, R.; Laio, A.; Parrinello, M. Predicting Crystal Structures: The Parrinello-Rahman Method Revisited. *Phys. Rev. Lett.* **2003**, *90* (7), 4.
- (27) Spoel, D. V. D.; Lindahl, E.; Hess, B.; Groenhof, G.; Mark, A. E.; Berendsen, H. J. C. GROMACS: Fast, Flexible, and Free. *J. Comput. Chem.* **2005**, *26* (16), 1701–1718.
- (28) GROMACS Documentation, Release 2021.2. 632.
- (29) Doherty, B.; Zhong, X.; Gathiaka, S.; Li, B.; Acevedo, O. Revisiting OPLS Force Field Parameters for Ionic Liquid Simulations. *J. Chem. Theory Comput.* **2017**, *13* (12), 6131–6145.
- (30) Jorgensen, W. L.; Maxwell, D. S.; Tirado-Rives, J. Development and Testing of the OPLS All-Atom Force Field on Conformational Energetics and Properties of Organic Liquids. *J. Am. Chem. Soc.* **1996**, *118* (45), 11225–11236.
- (31) Darden, T.; York, D.; Pedersen, L. Particle Mesh Ewald: An N-log(N) Method for Ewald Sums in Large Systems. *J. Chem. Phys.* **1993**, *98* (12), 10089–10092.
- (32) Williams, T.; Kelley, C. Gnuplot, An Interactive Plotting Program. [http://gnuplot.info/docs\\_5.5/gnuplot5.html](http://gnuplot.info/docs_5.5/gnuplot5.html) (accessed 2022–10–07).
- (33) *Grace User's Guide (for Grace-5.1.22)*. <https://plasma-gate.weizmann.ac.il/Grace/doc/UsersGuide.html> (accessed 2023–09–04).



- (34) Jiang, J.; Mei, Z.; Xu, J.; Sun, D. Effect of Inorganic Electrolytes on the Formation and the Stability of Water-in-Oil (W/O) Emulsions. *Colloids Surf, A* **2013**, *429*, 82–90.
- (35) Prieto, C.; Calvo, L. Performance of the Biocompatible Surfactant Tween 80, for the Formation of Microemulsions Suitable for New Pharmaceutical Processing. *Journal of Applied Chemistry* **2013**, *2013*, No. e930356.
- (36) Tantra, R.; Schulze, P.; Quincey, P. Effect of Nanoparticle Concentration on Zeta-Potential Measurement Results and Reproducibility. *Particuology* **2010**, *8* (3), 279–285.
- (37) Lowry, G. V.; Hill, R. J.; Harper, S.; Rawle, A. F.; Hendren, C. O.; Klaessig, F.; Nobbmann, U.; Sayre, P.; Rumble, J. Guidance to Improve the Scientific Value of Zeta-Potential Measurements in nanoEHS. *Environ. Sci.: Nano* **2016**, *3* (5), 953–965.
- (38) Al Shaal, L.; Shegokar, R.; Müller, R. H. Production and Characterization of Antioxidant Apigenin Nanocrystals as a Novel UV Skin Protective Formulation. *Int. J. Pharm.* **2011**, *420* (1), 133–140.
- (39) Nyepetsi, M.; Mbaiwa, F.; Oyetunji, O. A.; de Leeuw, N. H. Understanding the Interactions between Triolein and Cosolvent Binary Mixtures Using Molecular Dynamics Simulations. *ACS Omega* **2022**, *7* (12), 10212–10224.
- (40) Tai, A.; Bianchini, R.; Jachowicz, J. Texture analysis of cosmetic/pharmaceutical raw materials and formulations. *International Journal of Cosmetic Science* **2014**, *36* (4), 291–304.
- (41) Tafuro, G.; Costantini, A.; Baratto, G.; Busata, L.; Semenzato, A. Rheological and Textural Characterization of Acrylic Polymer Water Dispersions for Cosmetic Use. *Ind. Eng. Chem. Res.* **2019**, *58* (51), 23549–23558.
- (42) Hess, B. Determining the Shear Viscosity of Model Liquids from Molecular Dynamics Simulations. *J. Chem. Phys.* **2002**, *116* (1), 209–217.
- (43) Goodwin, J. W.; Hughes, R. W. *Rheology for Chemists – An Introduction*; Royal Society of Chemistry, 2008.
- (44) Steffe, J. F. *Rheological Methods in Food Process Engineering* (2nd ed.); Freeman Press, 1996.